Design of Zone-Based Hierarchical Protection System for 100% Renewable Microgrids

Preprint

Soham Chakraborty and Jing Wang

National Renewable Energy Laboratory

Presented at the 2024 IEEE PES T&D Conference & Exposition
Anaheim, California
May 6–9, 2024

NREL is a national laboratory of the U.S. Department of Energy
Office of Energy Efficiency & Renewable Energy
Operated by the Alliance for Sustainable Energy, LLC

This report is available at no cost from the National Renewable Energy Laboratory (NREL) at www.nrel.gov/publications.

Contract No. DE-AC36-08GO28308

Conference Paper
NREL/CP-5D00-87200
June 2024

Design of Zone-Based Hierarchical Protection System for 100% Renewable Microgrids

Preprint

Soham Chakraborty and Jing Wang

National Renewable Energy Laboratory

Suggested Citation
Chakraborty, Soham, and Jing Wang. 2024. *Design of Zone-Based Hierarchical Protection System for 100% Renewable Microgrids: Preprint*. Golden, CO: National Renewable Energy Laboratory. NREL/CP-5D00-87200.
https://www.nrel.gov/docs/fy24osti/87200.pdf.

NREL is a national laboratory of the U.S. Department of Energy
Office of Energy Efficiency & Renewable Energy
Operated by the Alliance for Sustainable Energy, LLC

This report is available at no cost from the National Renewable Energy Laboratory (NREL) at www.nrel.gov/publications.

Contract No. DE-AC36-08GO28308

Conference Paper
NREL/CP-5D00-87200
June 2024

National Renewable Energy Laboratory
15013 Denver West Parkway
Golden, CO 80401
303-275-3000 • www.nrel.gov

NOTICE

This work was authored by the National Renewable Energy Laboratory, operated by Alliance for Sustainable Energy, LLC, for the U.S. Department of Energy (DOE) under Contract No. DE-AC36-08GO28308. This work was supported by the Laboratory Directed Research and Development (LDRD) Program at NREL. The views expressed herein do not necessarily represent the views of the DOE or the U.S. Government.

Cover Photos by Dennis Schroeder: (clockwise, left to right) NREL 51934, NREL 45897, NREL 42160, NREL 45891, NREL 48097, NREL 46526.

Design of Zone-Based Hierarchical Protection System for 100% Renewable Microgrids

Soham Chakraborty, Jing Wang
Power Systems Engineering Center, National Renewable Energy Laboratory, Golden, Colorado 80401, USA.
{soham.chakraborty, jing.wang}@nrel.gov

***Abstract*—Design of a reliable and secure protection system for a 100% renewable microgrid with only inverter-based resources (IBRs) is quite challenging. Most existing protection schemes reflecting the current state of the art are suitable for microgrids with mixed types of distributed energy resources (DERs), including both rotating machine-based DERs as well as IBR-based DERs, where the fault current level is moderately high. Due to the drastic reduction in the fault current level of IBRs, the existing protection schemes face critical challenges in a 100% renewable microgrid. To address these fundamental challenges, this article proposes a zone-based hierarchical protection scheme that partitions a microgrid into various zones of protection and assigns speed-based hierarchical protection schemes. The performance of the proposed scheme is evaluated using a time-domain simulation study on a microgrid test system. The results corroborate that the proposed hierarchical zone-based protection scheme exhibits good reliability, security, and dependability when tested with various fault cases (fault types, locations, and impedances) and non-fault cases during both grid-tied and islanded mode.**

I. Introduction

Ensuring the protection of microgrids is the most critical challenge to be resolved to ensure their reliable and safe operation [1]. The protection of microgrids has been a complex and pivotal issue for researchers both in industry and academia due to their unique and dynamic characteristics compared with distribution systems. Several proposals have been made to provide an appropriate strategy that is capable of protecting microgrid in both modes. A communication-assisted differential protection scheme is proposed in [2]. Although it has a high dependability, this scheme faces serious security issues caused by un-synchronized data gathering due to communication delays and package drop issues to the transmitted signals. Adaptive settings for directional overcurrent relays (DOCRs) based on the mode of operation have been proposed [3], [4]. Practical challenges related to these schemes are well studied in [5], [6], which proposes a microprocessor-based, adaptive DOCR coordinated protection strategy and a positive-negative sequence superimposed current-based overcurrent relaying technique. The main drawback is the sensitivity issues introduced by the large reduction in the fault current levels and the failure of the directional elements due to the unconventional nature and power factor of the fault current contribution from inverter-based resources (IBRs) [7]. An admittance relay-based protection strategy is proposed in [8]. The ambiguity in the operation of the IBRs during an unbalanced fault can adversely affect the admittance/impedance calculation and could be proven ineffective for short lines where it is difficult to discriminate between in-zone and out-of zone faults. A hybrid tripping characteristics-based communication-less DOCR protection scheme is proposed in [9]–[11]. Although these schemes reduce the cost of the protection system, the implementation and the design of the relay coordination with these unconventional relay characteristics are challenging [3].

Most research efforts, however, focus on microgrids with mixed-type distributed energy resources (DERs), including rotating machine-based DERs, such as diesel generation sets; gas turbine resources; and IBR-based DERs, such as photovoltaic (PV)-based grid-following (GFL) IBRs, and battery energy storage system (BESS)-based grid-forming (GFM) IBRs. In the emerging 100% renewable microgrids, the main challenge, especially during islanded mode, is the low fault current contributions by the IBRs, which are restricted by the current ratings of the switches and the fault-limiter settings of the IBRs. The drastic reduction in the fault current level could result in either a complete failure to pick up or a delayed tripping by conventional protection systems. Moreover, 100% renewable microgrids might have varying operating levels of IBR-based DERs due to variability of the renewable resources. This has a direct influence on the level of the low fault current and eventually impacts on the conventional threshold-based protection system and relay coordination. Therefore, the development of a protection system that will suffice for both operating modes and varying IBR operations is a challenging task and remains an open research topic. This article proposes a secure and reliable zone-based hierarchical protection scheme, which can be used as design and implementation guidelines for the 100% renewable microgrids. The main contributions of the article are:

- This paper introduces a design methodology to partition the microgrid into multiple zones based on the elements of the circuit (lines, buses etc.) regardless of the topology.
- Based on the distinct features of different protection zones, unique protection schemes are employed for each zone for the best reliability, selectively and sensitivity.
- A hierarchical structure is designed for the protection system that enables the relay coordination by assigning different speeds of the protection systems to different zones.

This work was authored by the National Renewable Energy Laboratory (NREL), operated by Alliance for Sustainable Energy, LLC, for the U.S. Department of Energy (DOE) under Contract No. DE-AC36-08GO28308. This work was supported by the Laboratory Directed Research and Development (LDRD) Program at NREL. The views expressed in the article do not necessarily represent the views of the DOE or the U.S. Government. The U.S. Government retains and the publisher, by accepting the article for publication, acknowledges that the U.S. Government retains a nonexclusive, paid-up, irrevocable, worldwide license to publish or reproduce the published form of this work, or allow others to do so, for U.S. Government purposes.

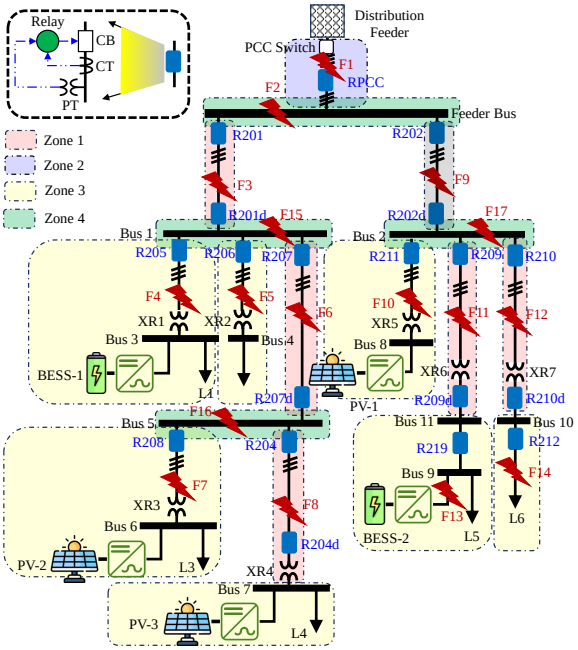

Fig. 1. Microgrid network and the protection system under study.

The simulation results corroborate that the proposed hierarchical zone-based protection scheme exhibits good reliability, security, and dependability for a 100% renewable microgrid during both grid-tied and islanded mode.

II. Proposed Zone-Based Hierarchical Protection

An example microgrid is selected based on Feeder 2 of the Banshee distribution benchmark system [12]. The original distribution network has 1 BESS (BESS-1) of 2.5-MVA rating and 1 PV IBR (PV-1) of 2-MW rating, connected to Bus-1 and Bus-8, respectively, as shown in Fig. 1. To convert the network into a 100% renewable microgrid, BESS-2 of 1-MVA rating at Bus-9, PV-2 of 0.5-MW at Bus-6, and PV-3 of 1-MW at Bus-7 are added. The BESS are operating with GFM control (power tracking for grid-connected mode and VF power sharing control for islanded mode). The PV units are operating in GFL control while following three modes: i) fixed power factor, ii) P-Q dispatch, and iii) volt-volt ampere reactive control. Both the BESS and the PV IBR responses to abnormal voltages and the voltage ride-through capabilities comply with IEEE 1547-2018 Category III [13]. More details about the ratings of various buses, loads, and the transformers can be found in [12]. The proposed hierarchical zone-based protection scheme, as shown in Fig. 1, is described next.

A. Protection System for Zone-1

Zone-1, as shown in Fig. 1, includes all the feeder line zones, where the ZoP is the line connecting two feeder buses, e.g., the line between the feeder bus and Bus-1, the feeder bus and Bus-2, etc. The line differential protection schemes are used to protect the ZoPs, as shown in Fig. 2. Two relays, 87L, are connected across the line between Bus-m and Bus-n. The equivalent electrical circuit and the current flow during

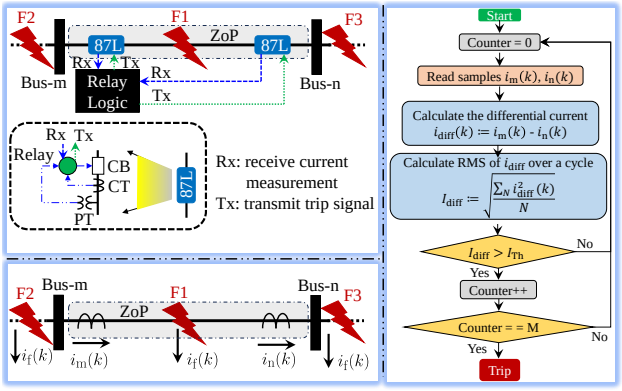

Fig. 2. Line differential-based protection scheme for Zone-1 of the microgrid.

the faults are shown at the bottom of Fig. 2. In the non-fault and fault F2 and F3, $i_m(k) - i_n(k) = 0$, and during only fault F1, $i_m(k) - i_n(k) = i_f(k) > 0$, where, $i_m(k)$, $i_n(k)$, and $i_f(k)$ are the k^{th} sample of the current measured by relays at Bus-m and Bus-n and the fault current, respectively. The algorithm flowchart of the protection scheme is shown at the right side of Fig. 2. In a real-world scenario, for faults outside the ZoP, $i_m(k) - i_n(k)$ will be nonzero but small due to different CT characteristics, CT saturation levels, delays in the communication channel, etc. [14]. I_{Th} is judiciously designed for satisfactory reliability as follows: $I_{Th} = \alpha \times \sqrt{2} I_{rated} \sin[2\pi(n+D)/N]$. α is the CT saturation factor, which can be found in the CT specification according to IEEE C37.110-2007 [15], I_{rated} is the rated line current of the ZoP, N is the number of samples in each cycle, and n signifies the n^{th} sample index. D is the sample delay in communication. To avoid nuisance tripping, a condition hold (Counter=M) is applied to negate the false fault-like situations. In this study, α, N, D, and M are selected as 2, 100, 2, and 200, respectively.

B. Protection System for Zone-2 and Zone-3

Zone-2 is the main feeder line of the microgrid, as shown in Fig. 1. Zone-3, also called a load-generation zone, includes the areas upstream of the load/generation point of connection and downstream of the nearest feeder bus, as shown by the yellow in Fig. 1. The protection schemes are as follows:

- Zone-2 : If the microgrid is in grid-tied mode and F1 of Fig. 1 is upstream of RPCC, the fault current sensed by RPCC is supplied by all downstream IBRs. If F1 is downstream of RPCC, then the fault current sensed by RPCC is supplied by the distribution grid. But if the microgrid is in islanded mode and F1 is upstream of RPCC, the fault current sensed by RPCC is supplied by all downstream IBRs, and if F1 is downstream of RPCC, the fault current sensed by RPCC is zero. As a result, an adaptive directional voltage-restrained overcurrent (VR-OC) protection is suitable here.
- Zone-3 : Irrespective of the operational mode of the microgrid, relays in Zone-3 will only operate if the faults are downstream of the relays. For example, if F4 is downstream of R205, the fault current sensed by R205 is supplied by all upstream IBRs, and the grid (depending on the mode) and the

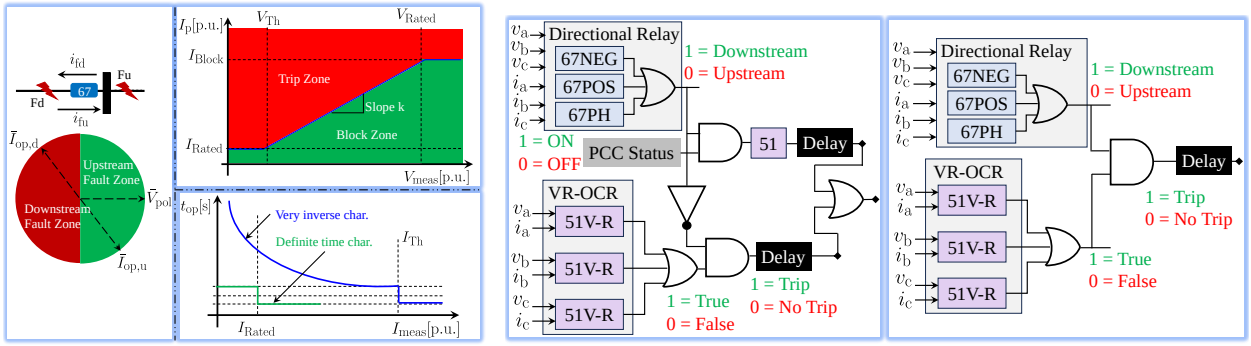

(a) (b)

Fig. 3. Protection scheme for Zone-2 and Zone-3 of the microgrid with (a) adaptive directional voltage-restrained overcurrent relays and (b) a logic diagram.

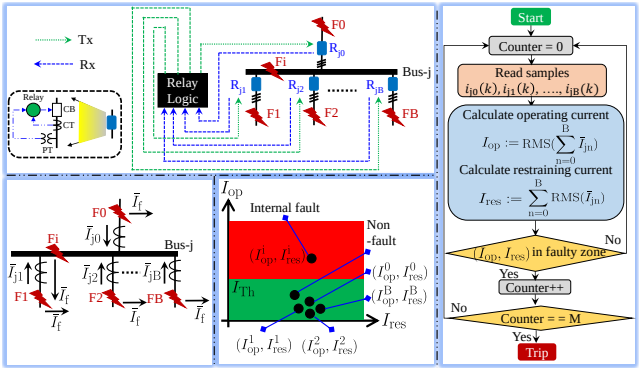

Fig. 4. Zone-4 protection scheme based on operating-restraining phenomenon.

relay should trip. If F4 is upstream of R205, it should not trip because it is situated in either of the other zones. Therefore, a directional VR-OC protection is most suitable here.

For both schemes, the directional element is the key element that is common. In this work, we use voltage-polarized directional elements [16], as shown in the leftmost figure of Fig. 3(a). Based on the positive/negative value of the computed hypothetical torque, $T_{\text{dir}} := |\bar{V}_{\text{pol}}||\bar{I}_{\text{op}}|\cos(\angle\bar{V}_{\text{pol}} - \angle\bar{I}_{\text{pol}})$, an upstream/downstream fault with respect to a relay can be detected. In this work, we use a combination of *negative-sequence* (67NEG), *positive-sequence* (67POS), and *phase* (67PH) directional elements. VR-OC is the second element in this protection scheme. VR-OC decides the setting of the pickup current, I_{p}, for the overcurrent relay based on the measured voltage, V_{meas}, by the relay. I_{p} of the VR-OC relay is a function of the fault voltage, as shown in Fig. 3(a). The definite-time overcurrent characteristic, with $t_{\text{op}} = 5$ cycles, is desirable for Zone-3 protection due to the low amount of fault current, especially during islanded mode. In this work, for Zone-2, we use an adaptive selection between a very-inverse-time overcurrent relay characteristic during grid-tied conditions with a downstream fault and a VR-OC relay characteristic for all other situations [15]. The relay logic for Zone-2 and Zone-3 are shown on the left and right sides of Fig. 3(b), respectively. The setting parameters are required to be judiciously designed for satisfactory reliability, and in this study, I_{Block}, V_{Th} are selected as 4 times and 25% of the rated line current and voltage, respectively. Standard parameters of very-inverse overcurrent characteristics with I_{p} computed by *short-circuit-ratio* value are used.

C. Protection System for Zone-4

Zone-4, as shown in Fig. 1, includes all the feeder buses, where the ZoP is the corresponding buses. A modified restrained differential scheme is used to protect the ZoP (i.e., Bus-j of Fig. 4) by detecting inside the ZoP faults (e.g., Fi of Fig. 4) and outside the ZoP faults (e.g., F0, F1, F2,.., FB of Fig. 4), sensed and tripped by all the relays (e.g., relay R_{j0}, R_{j1}, R_{j2},.., and R_{jB} of Fig. 4) [17]. The equivalent electrical circuit and the current flow during faults are shown at the bottom left of Fig. 4. Nodal current at Bus-j during all external faults as well as the normal no-fault situation would be zero and non-zero during inside fault, according to Kirchhoff's current law. Based on this, the operating current, $I_{\text{op}} := \text{RMS}(\sum_{\text{n=0}}^{\text{B}} \bar{I}_{\text{jn}})$, and the restraining current, $I_{\text{res}} := \sum_{\text{n=0}}^{\text{B}} \text{RMS}(\bar{I}_{\text{jn}})$, are defined as follows: where $\bar{I}_{\text{jn}}$ is the phasor current measured by relay R_{jn}. The quantity $(I_{\text{op}}, I_{\text{res}})$ will lie in the restraining zone (green area of the bottom middle figure of Fig. 4) in case of F0, F1, F2,.., FB. Whereas the quantity $(I_{\text{op}}, I_{\text{res}})$ will lie in the fault zone (red area of the bottom middle figure of Fig. 4) in case of only Fi. In this work, the slope of conventional differential restrain relay characteristics is considered to be zero. The line separating these zones, I_{Th}, is judiciously designed in this study based on practical non-idealities, such as CT saturation and communication delays, and it is expressed as: $I_{\text{Th}} := \alpha \times \max(I^{\text{r}}_{\text{j0}}, I^{\text{r}}_{\text{j1}}, \ldots, I^{\text{r}}_{\text{jB}})$. α is the CT saturation factor, which can be found in the CT specification according to IEEE C37.110-2007 [15]; and I^{r}_{jn} is the rated nodal current measured by the n^{th} relay. The algorithm flowchart of the protection scheme is shown on the right side of Fig. 4. To avoid nuisance tripping, a condition hold (Counter=M) is applied to negate the false fault-like situations. In this study, α and M are selected as 2 and 200, respectively.

VR-OC tripping characteristics is employed to the relays situated in Zone-1 and Zone-4 for backup protection system with proper relay coordination.

III. Time-Domain Simulation and Results

A MATLAB/Simulink-based time-domain simulation with a simulation time step of $T_{\text{s}} = 50\mu$s of the microgrid shown in

TABLE I
Performance of the Proposed Zone-Based Hierarchical Protection Scheme

Mode	Rel.	Dep.	Sec.
Grid-tied	98.26	98.12	98.27
Islanded	97.77	97.63	97.78
Overall	98.00	97.89	98.02

Mode	Speed [s]	
	max.	min.
Grid-tied	0.033	0.27
Islanded	0.033	0.32

Rel. : Reliability[%], Dep. : Dependability[%], Sec. : Security[%]

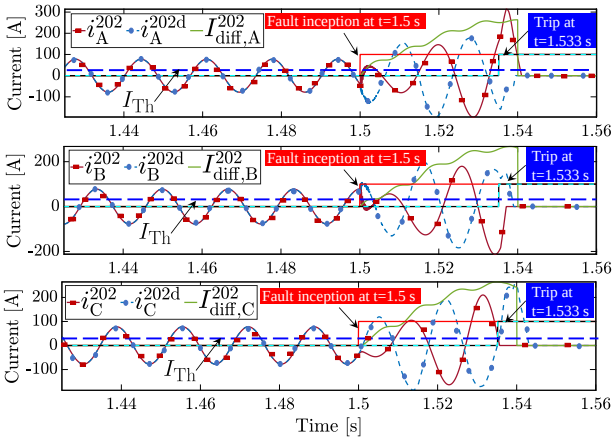

Fig. 5. Results during a fault, ABCg, with fault resistance of $R_{\rm f} = 0.5\Omega$ at location F9 while the microgrid is operating in islanded mode.

Fig. 1 with the proposed protection scheme is conducted. In total, 1620 cases are simulated with 1150 *fault* cases covering various fault types, locations, and impedances and 470 *fault-like* cases, such as large load/capacitor bank switching, solar irradiance drop/rise, and induction motor inrush. A birds-eye view of the performance of the proposed protection scheme is shown in Table I. The proposed protection system exhibits good performance on the basis of high reliability, dependability, and security ($> 97\%$). Moreover, due to the zone-based hierarchical protection scheme, the speed of the protection system also lies between 2 cycles (0.033s) and ≈ 20 cycles (0.32s). Table II shows a few results of the proposed scheme during few selected fault cases. It is observed that the proposed protection scheme can correctly enable the relays to trip the faulty circuit to localize and isolate the fault. Note that the IBR's own IEEE 1547-2018 Category III-compliant fault ride-through capability is also part of the results for completely isolating the fault from the healthy portion of the circuit. For example, in fault cases such as F4, F7, F10, F13, along with the relays of the network, breakers related to various IBRs are also operating to isolate the corresponding faults.

Fig. 5 shows the results of the performance of the protection system during a three-phase-to-ground fault (ABCg) with fault resistance of $R_{\rm f} = 0.5\Omega$ at location F9 while the microgrid is operating in islanded mode. The fault occurred at $t = 1.5$s , and the figure shows that the $I^{202}_{\rm diff,A}$, $I^{202}_{\rm dif,B}$, and $I^{202}_{\rm diff,C}$, as defined in Fig. 2, jumped from their pre-fault values, which are very low and less than the $I_{\rm Th}$, to a high value and crossed the thresholds. As a result, after the waiting period of 2 cycles (M = 200 of Fig. 5), the relays, R202 and R202d, generate the corresponding trip signals at $t = 1.533$ s.

Fig. 6 shows the results of the performance of the protection

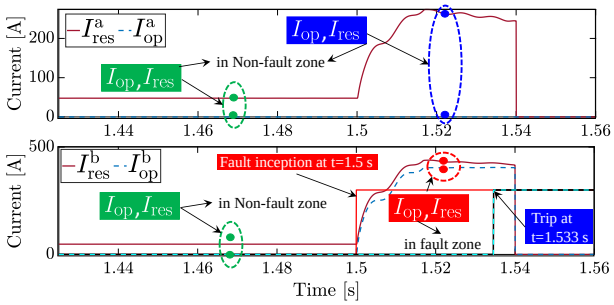

Fig. 6. Results during a fault, Bg, with fault resistance of $R_{\rm f} = 10\Omega$ at location F2 while the microgrid is operating in grid-tied mode.

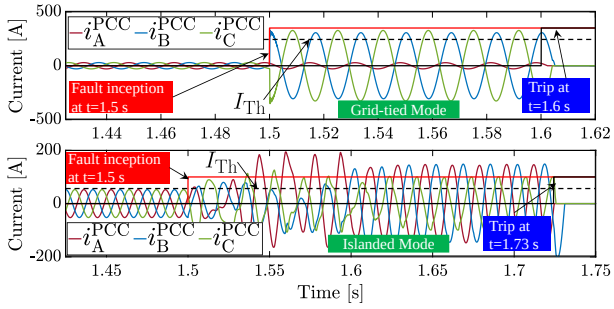

(a)

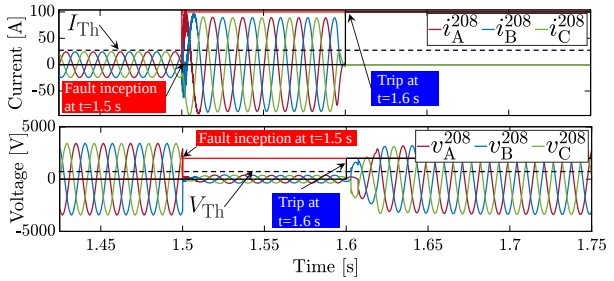

(b)

Fig. 7. Results during a fault, (a) CA, with fault resistance of $R_{\rm f} = 0.01\Omega$ at location F1, downstream during grid-tied mode and upstream during islanded mode, and (b) ABCg, with fault resistance of $R_{\rm f} = 3\Omega$ at location F7.

system during a single-line-to-ground fault (Bg) with fault resistance of $R_{\rm f} = 10\Omega$ at location F2 while the microgrid is operating in grid-tied mode. The fault occurred at $t = 1.5$s, and the figure shows that the $I_{\rm op}$ and $I_{\rm res}$, calculated in phase-b, lie in the non-fault zone and the fault zone of Fig. 4 before and after the fault inception, respectively. Whereas $I_{\rm op}$ and $I_{\rm res}$, calculated in phase-a, always lie in the non-fault zone of Fig. 4. As a result, after the waiting period of 2 cycles (M = 200 of Fig. 6), the relays, RPCC, R201, and R202, generate the corresponding trip signals at $t = 1.533$s.

Fig. 7(a) shows the results of the performance of the protection system during a line-to-line fault (CA), which occurred at $t = 1.5$ s, with fault resistance of $R_{\rm f} = 0.01\Omega$ at location F1, downstream of RPCC in grid-tied mode and upstream of RPCC in islanded mode. During the grid-tied condition, the relay, RPCC, detects the downstream fault, and the relay adapts the very-inverse tripping overcurrent characteristics and trips at $t = 1.6$ s. Whereas during islanded

TABLE II
Operating time of the relays for the selected faults on the test system of Fig. 1 for both grid-tied (G) and islanded (I) mode.

Type	F1(G) (ag) 0.01Ω	F2(I) (abcg) 25Ω	F3(G) (bg) 15Ω	F4(I) (cg) 1Ω	F5(G) (bg) 2Ω	F6(I) (abc) 20Ω	F7(G) (ag) 0.05Ω	F8(I) (bg) 10Ω	F9(G) (cg) 30Ω	F10(I) (acg) 0.01Ω	F11(G) (bc) 5Ω	F12(I) (ag) 8Ω	F13(G) (bg) 3Ω	F14(I) (bcg) 2.5Ω	F15(G) (ac) 10Ω	F16(I) (bg) 25Ω	F17(G) (ag) 5Ω
Relay	RPCC, PCC −switch	RPCC, R201, R202	R201, R201d	R205, BESS1 −switch	R206	R207, R207d	R208, PV2 −switch	R204, R204d	R202, R202d	R211, PV1 −switch	R209, R209d	R210, R210d	R219, BESS2 −switch	R212	R201d, R205, R206, R207	R207d, R208, R204	R202d, R209, R210, R211
Time[s]	0.17	0.033	0.033	0.21	0.09	0.033	0.19	0.033	0.033	0.18	0.033	0.033	0.17	0.11	0.033	0.033	0.033

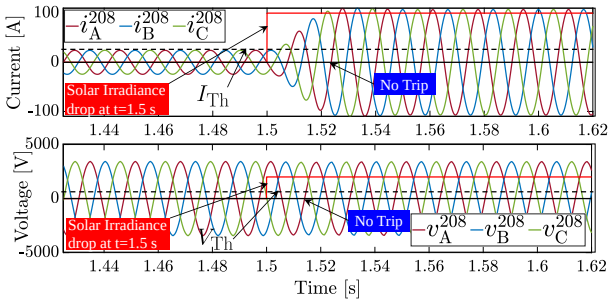

Fig. 8. Results during fault-like cases, such as a drop in solar irradiance in all the PV IBRs from rated to 10% seen by R208, in islanded mode.

mode, RPCC detects the upstream fault, and the relay adapts the VR-OC characteristics and trips at $t = 1.73$ s. Fig. 7(b) shows the results of the performance of the protection system during a three-phase-to-ground fault (ABCg), which occurred at $t = 1.5$ s, with fault resistance of $R_f = 3\Omega$ at location F7, while the microgrid is operating in islanded mode. Relay R208 operates with the VR-OC characteristics by measuring the low voltage across the relay and determines the I_{Th} based on Fig. 3(a). As a result, the relay trips at $t = 1.6$ s.

Fig. 8 shows the performance of the protection scheme during the drop in solar irradiance in all the PV IBRs from rated to 10% for the islanded microgrid. Zone-1 and Zone-4 protection do not operate because the relays will operate only when there is a fault inside the ZoP. The results show the performance of the sensitivity of the Zone-3 protection scheme with R208. It is observed that the current measurements are much larger than the rated current; however, because the voltage magnitudes are close to rated, the threshold current value becomes I_{Block}, as shown in Fig. 3(a). As a result, the VR-OC does not satisfy the current threshold logic, which leads to no tripping by R208.

IV. Conclusion

This paper proposes a new protection scheme to address the challenges of the state-of-the-art. A microgrid under study is partitioned into various ZoPs and then assigned speed-based hierarchical protection schemes that includes differential current-based line protection, restraining phenomenon-based bus protection, and VROC-based feeder protection. Based on the results showing the performance using a time-domain simulation study, it can be concluded that the proposed protection scheme exhibits good reliability, security, and dependability when it is employed in such a 100% renewable microgrid. Improving the operating time of the protection schemes, however, especially for Zone-3, is considered for future work to further enhance the proposed protection scheme. The guidelines of designing protection system presented in this paper can be applied for all the 100% renewable microgrids.

References

[1] A. Hooshyar and R. Iravani, "Microgrid protection," *Proceedings of the IEEE*, vol. 105, no. 7, pp. 1332–1353, 2017.

[2] E. Sortomme, S. Venkata, and J. Mitra, "Microgrid protection using communication-assisted digital relays," *IEEE Transactions on Power Delivery*, vol. 25, no. 4, pp. 2789–2796, 2009.

[3] L. Che, M. E. Khodayar, and M. Shahidehpour, "Adaptive protection system for microgrids: Protection practices of a functional microgrid system," *IEEE Electrification magazine*, vol. 2, no. 1, pp. 66–80, 2014.

[4] D. Lagos, V. Papaspiliotopoulos, G. Korres, and N. Hatziargyriou, "Microgrid protection against internal faults: Challenges in islanded and interconnected operation," *IEEE Power and Energy Magazine*, vol. 19, no. 3, pp. 20–35, 2021.

[5] M. A. Zamani, T. S. Sidhu, and A. Yazdani, "A protection strategy and microprocessor-based relay for low-voltage microgrids," *IEEE transactions on Power Delivery*, vol. 26, no. 3, pp. 1873–1883, 2011.

[6] H. Muda and P. Jena, "Superimposed adaptive sequence current based microgrid protection: A new technique," *IEEE Transactions on Power Delivery*, vol. 32, no. 2, pp. 757–767, 2016.

[7] K. Saleh, M. A. Allam, and A. Mehrizi-Sani, "Protection of inverter-based islanded microgrids via synthetic harmonic current pattern injection," *IEEE Transactions on Power Delivery*, vol. 36, no. 4, pp. 2434–2445, 2020.

[8] M. Dewadasa, A. Ghosh, G. Ledwich, and M. Wishart, "Fault isolation in distributed generation connected distribution networks," *IET generation, transmission & distribution*, vol. 5, no. 10, pp. 1053–1061, 2011.

[9] S. Chakraborty and S. Das, "Communication-less protection scheme for ac microgrids using hybrid tripping characteristic," *Electric Power Systems Research*, vol. 187, p. 106453, 2020.

[10] A. Darabi, M. Bagheri, and G. B. Gharehpetian, "Highly sensitive microgrid protection using overcurrent relays with a novel relay characteristic," *IET Renewable Power Generation*, vol. 14, no. 7, pp. 1201–1209, 2020.

[11] W. T. El-Sayed, M. A. Azzouz, H. H. Zeineldin, and E. F. El-Saadany, "A harmonic time-current-voltage directional relay for optimal protection coordination of inverter-based islanded microgrids," *IEEE Transactions on Smart Grid*, vol. 12, no. 3, pp. 1904–1917, 2020.

[12] J. Wang, "Study of inverter control strategies on the stability of microgrids toward 100% renewable penetration," in *IECON 2022–48th Annual Conference of the IEEE Industrial Electronics Society*. IEEE, 2022, pp. 1–5.

[13] "IEEE standard for interconnection and interoperability of distributed energy resources with associated electric power systems interfaces," *IEEE Std 1547-2018 (Revision)*, pp. 1–138, 2018.

[14] P. Liu, B. Jiao, P. Zhang, S. Du, J. Zhu, and Y. Song, "Countermeasure to prevent transformer differential protection from false operations," *IEEE Access*, 2023.

[15] "IEEE standard for ratings and requirements for ac high-voltage circuit breakers with rated maximum voltage above 1000 v," *IEEE Std C37.04-2018 (Revision of IEEE Std C37.04-1999)*, pp. 1–122, 2019.

[16] A. Hooshyar and R. Iravani, "A new directional element for microgrid protection," *IEEE Transactions on Smart Grid*, vol. 9, no. 6, pp. 6862–6876, 2018.

[17] R. Rifitat, "Considerations in applying power bus protection schemes to industrial and ipp systems," in *Conference Record of the 2002 IEEE Industry Applications Conference. 37th IAS Annual Meeting (Cat. No.02CH37344)*, vol. 3, 2002, pp. 2231–2237 vol.3.